# Electronic band structures of group-IV two-dimensional materials: Spin-orbit coupling and group theoretical analysis

# Electronic band structures of group-IV two-dimensional materials: Spin-orbit coupling and group theoretical analysis

Salsabila Amanda Putri[a], Yuki Yamaguchi[a], Thomas Aquino Ariasoca[a], Muhammad Yusuf Hakim Widianto[a,c,*], Katsunori Tagami[b], Mineo Saito[c]

[a]*Graduate School of Natural Science and Technology, Kanazawa University, Kanazawa 920-1192, Japan*
[b]*ASMS Co., Ltd., Shinagawa, Tokyo 141-0022, Japan*
[c]*Faculty of Mathematics and Physics, Institute of Science and Technology, Kanazawa University, Kanazawa 920-1192, Japan*

## Abstract

Band structures of group-IV two-dimensional materials are studied by carrying out first-principles calculations including spin-orbit coupling (SOC). We propose a method that identifies irreducible representations (IR) of bands by using computers. We identify IR for the planar and buckled structures and discuss the difference between bands obtained by non-SOC and SOC calculations. In particular, we clarify IR at the Dirac point where the bands split because of the SOC. We evaluate the $Z_2$ invariants based on identified IR, which suggests that all the systems are topological insulators.

*Keywords:* Electronic structures, Spin-Orbit Coupling, Group Theory

## 1. Introduction

Two-dimensional materials have been attracting scientific interests because of their novel electronic properties. Since the discovery of graphene in 2004[1, 2], hexagonal group-IV materials including silicene[3, 4, 5], germanene[6], and stanene[7] have been extensively studied. In particular, the Dirac cones in the electronic band structure characterize the electronic properties of these materials[8, 9, 10].

The spin-orbit coupling (SOC) splits the bands at the Dirac point[11]. Because of this band split, graphene is considered to become a topological insulator though the band gap is very small[12]. The SOC becomes large as the atom becomes heavy, so other group-IV materials are good candidates for $Z_2$ topological insulators[13, 14, 15].

---

*Corresponding author

*Email address:* `mwidianto@cphys.s.kanazawa-u.ac.jp` (Muhammad Yusuf Hakim Widianto)

In the field of spintronics, the SOC is expected to induce new functions in device materials. To deeply understand electronic properties, the analysis based on the double group theory is important. So far, irreducible representations (IR) in the double group have not been identified in most of cases. In the case of group-IV two-dimensional materials, there are some attempts to identify IR for the non-SOC bands[16, 17]. Some discussions on the SOC effect on the bands were done based on the group theory and tight binding models but little is known about IR of SOC bands[18, 19].

In this paper, we propose a method to identify IR of any $k$-point for the bands calculated from plane-wave base calculations and therefore the method can be applied to analysis of bands calculated from standard first-principles calculations. Since this method enables identification by using computers, we can avoid misidentification. We apply the method to analyze electronic structures of the group-IV two-dimensional materials and clarify the difference between the bands obtained from SOC and non-SOC calculations. In particular, we clarify details of the level split of the Dirac cones and evaluate the $Z_2$ invariant based on the group theory.

## 2. Method

We first introduce a method which identifies IR of wavefunctions obtained from SOC calculations. The method for non-SOC calculations was previously reported[16, 20, 21, 22, 23]. The symmetry operator $\hat{R}_m$ consists of the rotation, $\hat{C}_m$, and of the fractional translation, $\hat{\tau}_m$:

$$\hat{R}_m = \{\hat{C}_m \mid \hat{\tau}_m\}. \tag{1}$$

The present systems are symmorphic and the fractional translations are ($\hat{\tau}_m = 0$). We next introduce the two-component spinor Bloch wavefunction:

$$\Psi_{\vec{k}}^j = \alpha \psi_{\vec{k},j}^\alpha + \beta \psi_{\vec{k},j}^\beta, \tag{2}$$

where $\vec{k}$ and $j$ are the wavevector in the first Brillouin zone and the band index in the ascending order of energy, respectively. $\alpha$ and $\beta$ are eigenfunctions of the operator for the spin angular momentum in the $z$ direction and their eigenvalues are $\frac{\hbar}{2}$ and $-\frac{\hbar}{2}$, respectively. The two spin-dependent wavefunctions are expressed as:

$$\psi_{\vec{k},j}^{(\alpha,\beta)}(\vec{r}) = \frac{1}{\sqrt{NV}} \sum_u c_{\vec{k},j}^{(\alpha,\beta)}(\vec{G}_u) \ \exp[i(\vec{k} + \vec{G}_u) \cdot \vec{r}], \tag{3}$$

where $N$ and $V$ are the number of unit cells and the unit cell volume, respectively, and $\vec{G}_u$ and $c_j^{(\alpha,\beta)}(\vec{G}_u)$ are the $u$-th reciprocal lattice vector and a coefficient, respectively.

2

To identify the IR of the wave functions which have the $q$-th degeneracy, we evaluate the following expression:

$$Q^\gamma = \frac{1}{l} \sum_{j=p}^{p+q-1} \sum_m \chi^\gamma(\hat{C}_m)^* \left\langle \Psi_{\vec{k}}^j \mid \hat{C}_m \mid \Psi_{\vec{k}}^j \right\rangle, \tag{4}$$

where $l$ and $\chi^\gamma(\hat{C}_m)$ are the order of the group and the character of IR $\gamma$, respectively, and $m$ runs over the symmetry operations of the $k$ group. If the condition of $Q^\gamma = 1$ ($Q^\gamma = 0$) is satisfied, the wave functions belong (do not belong) to the $\gamma$-th IR. By combining Eqs. (2) - (4), we obtain:

$$Q^\gamma = \frac{1}{l} \sum_{j=p}^{p+q-1} \sum_m \sum_u \chi^\gamma(\hat{C}_m)^* \Big[ c_{\vec{k},j}^\alpha (\hat{C}_m \vec{G}_u - \vec{G}'_m)^* (D_{11}^m c_{\vec{k},j}^\alpha(\vec{G}_u) + D_{12}^m c_{\vec{k},j}^\beta(\vec{G}_u)) +$$

$$c_{\vec{k},j}^\beta (\hat{C}_m \vec{G}_u - \vec{G}'_m)^* (D_{21}^m c_{\vec{k},j}^\alpha(\vec{G}_u) + D_{22}^m c_{\vec{k},j}^\beta(\vec{G}_u)) \Big], \tag{5}$$

where the reciprocal lattice vector $\vec{G}'_m$ satisfies $\hat{C}_m \vec{k} = \vec{k} - \vec{G}'_m$ ($\vec{G}'_m = 0$ when the $k$-point is located inside the first Brillouin zone (FBZ)). The matrix $\mathbf{D}^m$ represents the rotation ($\hat{C}_m$) for spin functions, $\alpha$ and $\beta$:

$$\begin{bmatrix} D_{11}^m & D_{12}^m \\ D_{21}^m & D_{22}^m \end{bmatrix} = \begin{bmatrix} \cos(\theta_m/2) - iv_m \sin(\theta_m/2) & -i(\lambda_m - i\mu_m)\sin(\theta_m/2) \\ -i(\lambda_m + i\mu_m)\sin(\theta_m/2) & \cos(\theta_m/2) + iv_m \sin(\theta_m/2) \end{bmatrix}, \tag{6}$$

where $\theta_m$ is the rotation angle around the axis whose direction cosine is ($\lambda_m$, $\mu_m$, $v_m$) [24].

We implement the above algorithm in the first-principles calculation code PHASE/0[25]. The present method is applied to plane-wave base calculational methods, i.e, the ultrasoft pseudopotential[26] and projector augmented wave (PAW) methods[27] as well as the norm-conserving pseudopotential method[28]. In the cases of the former two methods, we apply Eq. (4) to the soft (plane-wave) part after the part is normalized. In this paper, we use Bethe[29] and Mulliken[30, 31] symbols to represent IR. In the case of Mulliken symbols for the double group, we use a notation of a reference[32]. We use character tables presented in a text book[24].

We carry out density functional theory (DFT) band structure calculations based on the generalized gradient approximation[33]. The slab models are used to simulate two-dimensional materials; a vacuum space of 30Å is introduced to avoid the interlayer interaction. The $k$-point mesh is 16×16×1. We use norm-conserving[28] or ultrasoft pseudopotentials[26] for non-SOC calculations and PAW method[27] for SOC calculations.

## 3. Results and discussion

### 3.1. Geometry optimization

We define the unit cell as shown in Fig. 1(a) and the FBZ is shown in Fig. 1(b). We optimize the lattice constant and internal coordinates by performing

DFT calculations without SOC (Table I) and find that graphene forms a planar structure and silicene, germanene, and stanene form buckled structures. As a result, graphene and the other group-IV materials belong to P6/mmm ($D_{6h}^1$) and P$\bar{3}$m1 ($D_{3d}^3$), respectively. The optimized lattice constant ($a$) and the buckling height ($h$) are comparable with those in previous calculations[34].

### 3.2. Graphene

We first study graphene by carrying out non-SOC calculation (Fig.2(a)). The Dirac point is located at the K point whose point group is $D_{3h}$. The two wavefunctions belong to a two-dimensional representation E'' ($K_6$) and thus the two wavefunctions have the identical energy[16].

When the SOC is included in band structure calculations, the E'' ($K_6$) level splits into the $E_{1/2}$ ($K_7$) and $E_{3/2}$ ($K_9$) levels according to the direct product:

$$E'' \ (K_6) \otimes E_{1/2} \ (K_7) = E_{1/2} \ (K_7) \oplus E_{3/2} \ (K_9), \tag{7}$$

where $E_{1/2}$ ($K_7$) on the left-hand side is the IR of the spin function. We find that the $E_{3/2}$ ($K_9$) level is lower than the $E_{1/2}$ ($K_7$) level and is occupied by two electrons (Fig. 2(b)). Because of this energy split, the system becomes an insulator. The energy split is very small and is less than 1 meV, which is consistent with past theoretical results[11, 12, 34, 35].

We next consider the $\Gamma$ point whose point group is $D_{6h}$. The highest occupied level calculated from non-SOC calculations is $E_{2g}$ ($\Gamma_6^+$) and the SOC splits it into $E_{5/2g}$ ($\Gamma_9^+$) and $E_{3/2g}$ ($\Gamma_8^+$) levels according to the direct product:

$$E_{2g} \ (\Gamma_6^+) \otimes E_{1/2g} \ (\Gamma_7^+) = E_{5/2g} \ (\Gamma_9^+) \oplus E_{3/2g} \ (\Gamma_8^+). \tag{8}$$

The $\Gamma_9^+$ level is found to be higher than that of the $\Gamma_8^+$ level.

The $k$-point group on the T, T′ and $\Sigma$ lines is $C_{2v}$. All the bands on these lines belong to ($E_{1/2}$ ($\Gamma_5$)). Therefore the bands do not cross on these lines (the second and third bands at a $k$-point on the T line have very close energies as Fig. 2(b) shows). On the other hand, bands belonging to different IR cross in the non-SOC calculations (Fig. 2(a)).

### 3.3. Tight binding model for graphene

As described in a previous subsection, the SOC splits the Dirac point into $E_{1/2}$ and $E_{3/2}$ levels and the former is higher than the latter. The suffix of E corresponds to the absolute value of the magnetic moment $|m_j|$ for the total angular momentum of the atomic spin-orbit wavefunction located at the original point. Therefore, it might be surprising that the $E_{3/2}$ level is higher than the $E_{1/2}$ level. Here, we discuss the reason for this energetical order based on a tight binding model.

Previous studies indicated that $d$ atomic orbitals mainly contribute to the energy split at the Dirac point[34, 36, 37]. We consider the Bloch wavefunctions consisting of the atomic orbitals ($p_z$, $d_1$, $d_{-1}$) for the A and B sublattices, where $d_1$ and $d_{-1}$ include the spherical harmonics, $Y_2^1$ and $Y_2^{-1}$, respectively,

i.e., $d_1 = -\frac{1}{\sqrt{2}}(d_{zx} + id_{yz})$ and $d_{-1} = \frac{1}{\sqrt{2}}(d_{zx} - id_{yz})$. According to Slater and Koster[38], two center integrals are given by $E_{z,zx} = lV_{pd\pi}$ and $E_{z,yz} = mV_{pd\pi}$ for the direction cosine $(l, m, 0)$. We here consider the Dirac electrons at the K′ point $(k = \frac{2\pi}{a}(\frac{2}{3}, 0))$. We obtain the hamiltonian matrix as:

$$
\begin{bmatrix}
E_p & -3(iV_{pd\pi})\varepsilon^*/\sqrt{2} & 0 \\
3(iV_{pd\pi})\varepsilon/\sqrt{2} & E_d & 0 \\
0 & 0 & E_d
\end{bmatrix},
\tag{9}
$$

for the basis subset A $(P_z^A, D_1^B, D_{-1}^B)$, and

$$
\begin{bmatrix}
E_p & 0 & 3(iV_{pd\pi})\varepsilon/\sqrt{2} \\
0 & E_d & 0 \\
-3(iV_{pd\pi})\varepsilon^*/\sqrt{2} & 0 & E_d
\end{bmatrix},
\tag{10}
$$

for the basis subset B $(P_z^B, D_1^A, D_{-1}^A)$, where $P_z^{A(B)}$, $D_1^{A(B)}$, and $D_{-1}^{A(B)}$ are the Bloch wavefunctions including atomic orbitals of $p_z^{A(B)}$, $d_1^{A(B)}$ and $d_{-1}^{A(B)}$ orbitals at the A (B) site, respectively. We define $\varepsilon = \exp(2\pi i/3)$. For example, $P_z^A$ is given by:

$$
P_z^A(r) = \frac{1}{\sqrt{N}} \sum_{n=1}^{N} \exp(i\vec{k} \cdot \vec{R}_n) p_z^A(r - \vec{R}_n),
\tag{11}
$$

where $N$ and $R_n$ are the number of the unit cell and the $n$-th lattice vector, respectively. All the matrix elements between the two wavefunctions belonging to different subsets are zero.

By using the second order perturbation theory, we obtain the energy at the Dirac cone as:

$$
E = E_p - \frac{9V_{pd\pi}^2/2}{E_d - E_p},
\tag{12}
$$

where $E_p$ and $E_d$ are the energies of the $p$ and $d$-orbitals, respectively. The wavefunctions are given by:

$$
\Psi_1 = P_z^A - \left[3(iV_{pd\pi})\varepsilon/\sqrt{2}\right]D_1^B/(E_d - E_p),
\tag{13}
$$

and

$$
\Psi_{-1} = P_z^B + \left[3(iV_{pd\pi})\varepsilon^*/\sqrt{2}\right]D_{-1}^A/(E_d - E_p).
\tag{14}
$$

These two wavefunctions belong to the E″ representation in the D$_{3h}$ symmetry.

We next consider the SOC by adding the perturbation to the Hamiltonian without non-spin orbit interaction. We introduce the atomic matrix elements $< m_1 m_{1/2} \mid \lambda \hat{l}_z \hat{s}_z \mid m_1 m_{1/2} >$ whose absolute value is $\zeta_d$, where $m_1$ and $m_{1/2}$ represent the magnetic quantum numbers of the $d$ orbital (1 or -1) and spin function (1/2 or -1/2). $\hat{l}_z$ ($\hat{s}_z$) is the operators for the $z$ component of the orbital (spin) angular momentum and $\lambda$ is a positive constant. These matrix

elements are considered to mainly contribute to the energy split of the Dirac cone. The amount of the split is approximately evaluated as:

$$\Delta E_{SO} \approx 9V_{pd\pi}^2 \frac{\zeta_d}{(E_d - E_p)^2}. \tag{15}$$

$\Psi_1(r)\alpha$ and $\Psi_{-1}(r)\beta$ have higher energies than $\Psi_1(r)\beta$ and $\Psi_{-1}(r)\alpha$ because the absolute values of the magnetic quantum numbers $d_1^B\alpha$ and $d_{-1}^A\beta$ ($|m_j| = 3/2$) are larger than those of $d_1^B\beta$ and $d_{-1}^A\alpha$ ($|m_j| = 1/2$). Here, we confirm that the Bloch wavefunctions, $\Psi_1(r)\alpha$ and $\Psi_{-1}(r)\beta$, belong to $E_{1/2}$ in spite of the fact that $|m_j|$ of the atomic orbitals, $d_1^B\alpha$ and $d_{-1}^A\beta$, are $3/2$. We also confirm that $\Psi_1(r)\beta$ and $\Psi_{-1}(r)\alpha$ belong to $E_{3/2}$ though $|m_j|$ of $d_1^B\beta$ and $d_{-1}^A\alpha$ are $1/2$.

Here, we confirm that the former two wavefunctions corresponding to $|m_j| = 3/2$ belong to $E_{1/2}$ and the latter two wavefunctions corresponding to $|m_j| = 1/2$ belong to $E_{3/2}$.

We find that

$$\hat{C}_3(\Psi_1\beta, \Psi_{-1}\alpha) = (\Psi_1\beta, \Psi_{-1}\alpha) \begin{bmatrix} -1 & 0 \\ 0 & -1 \end{bmatrix} \tag{16}$$

and

$$\hat{C}_3(\Psi_1\alpha, \Psi_{-1}\beta) = (\Psi_1\alpha, \Psi_{-1}\beta) \begin{bmatrix} \exp(i\pi/3) & 0 \\ 0 & \exp(-i\pi/3) \end{bmatrix}. \tag{17}$$

Therefore, the characters for the first two and latter two wavefunctions are -2 and -1, respectively, which is consistent with the fact that the former and latter basis sets belong to $E_{3/2}$ and $E_{1/2}$, respectively.

We discuss some details concerning Eqs. (16) and (17). The Bloch functions exemplified by Eq. (11) consist of $\exp(i\vec{k} \cdot \vec{R})$ and spin-orbit wavefunction. The rotation of $2\pi/3$ around the $z$ axis passing through the atomic site transforms spin-orbit wavefunctions $\phi_{m_j}$ into $(\varepsilon^*)^{m_j}\phi_{m_j}$ where the $m_j$ is the magnetic quantum number. When the rotation of $2\pi/3$ around the $z$ axis passing through the original point in the periodic system, $\hat{C}_3$, operates Bloch function, the term $\exp(i\vec{k}\cdot\vec{R})$ in the Bloch function gets the factor of $(\varepsilon^*)^{-1}$ and $\varepsilon^*$ for the A and B sites, respectively, as Fig. 3 shows. Therefore, $P_z^A\alpha$ and $D_1^B\alpha$ correspond to the states of $m_j = -1/2$ and $m_j = 5/2$, respectively, i.e., $\hat{C}_3 P_z^A\alpha = (\varepsilon^*)^{-1/2}P_z^A\alpha$ and $\hat{C}_3 D_1^B\alpha = (\varepsilon^*)^{5/2}D_1^B\alpha$. Since $m_j$ and $m_j \pm 3$ give the same value of $(\varepsilon^*)^{m_j}$, $m_j = -1/2$ and $m_j = 5/2$ give the same value. As a result, $\Psi_1(r)\alpha$ corresponds to the state of $m_j = -1/2$, i.e., $\hat{C}_3\Psi_1(r)\alpha = (\varepsilon^*)^{-1/2}\Psi_1(r)\alpha$. In a similar way, we find that $\hat{C}_3\Psi_{-1}\beta = (\varepsilon^*)^{1/2}\Psi_{-1}\beta$. The above results are consistent with the fact that $\Psi_1\alpha$ and $\Psi_{-1}\beta$ belong to $E_{1/2}$[39].

In a similar way to the above, we find that $\hat{C}_3 P_z^A\beta = (\varepsilon^*)^{-3/2}P_z^A\beta$, $\hat{C}_3 D_1^B\beta = (\varepsilon^*)^{3/2}D_1^B\beta$, $\hat{C}_3 P_z^B\alpha = (\varepsilon^*)^{3/2}P_z^B\alpha$ and $\hat{C}_3 D_{-1}^A\alpha = (\varepsilon^*)^{-3/2}D_{-1}^A\alpha$. Since $(\varepsilon^*)^{3/2} = (\varepsilon^*)^{-3/2} = -1$, we conclude that $\hat{C}_3\Psi_1\beta = -\hat{C}_3\Psi_1\beta$ and $\hat{C}_3\Psi_{-1}\alpha = -\hat{C}_3\Psi_{-1}\alpha$. These results are consistent with the fact that the two functions belong to $E_{3/2}$.

As mentioned above, the term $\exp(i\vec{k} \cdot \vec{R}_n)$ in the Bloch functions affects the identification of IR of Bloch functions, which leads to the fact that the $E_{3/2}$ level is lower than the $E_{1/2}$ level. In the case of the $\Gamma$ point, $\exp(i\vec{k} \cdot \vec{R}_n)$ does not affect the identification since $\exp(i\vec{k} \cdot \vec{R}_n) = 1$.

### 3.4. Silicene, germanene and stanene

We find that the buckled structure is the most stable in the cases of silicene, germanene, and stanene. The Dirac point is located at the K point whose point group is $D_3$ which is lower than $D_{3h}$ in the case of graphene. The two wavefunctions belong to a two-dimensional representation E and thus the two wavefunctions have the identical energy as Fig. 4 shows.

When the SOC is included in band calculations (Fig. 4), the E ($K_3$) level splits the level according to the direct product:

$$E \ (K_3) \otimes E_{1/2} \ (K_6) = e_{3/2}(1) \ (K_4) \oplus e_{3/2}(2) \ (K_5) \oplus E_{1/2} \ (K_6), \qquad (18)$$

where $K_5$ and $K_4$ are one-dimensional representation and the two levels have the same energy due to the time-reversal symmetry. Although these two representations are one-dimensional, they are represented by $E_{3/2}$ in the Mulliken symbols. Therefore, to avoid ambiguity, we introduce symbols $e_{3/2}(1)$ and $e_{3/2}(2)$ to represent $K_4$ and $K_5$, respectively.

We find that the $K_6$ level is higher than the $K_5$ and $K_4$ levels and $K_5$ and $K_4$ are occupied by electrons. Because of this energy split, the system becomes an insulator. The energy split becomes large as the atom becomes heavy (2 meV, 40 meV and 135 meV for silicene, germanene and stanene, respectively). This chemical trend is consistent with past theoretical results[34, 40, 41]. The calculated SOC band gaps of the group-IV materials are tabulated in Table 1. The valence band top is located at the K point except for stanene where the top is located at the $\Gamma$ point. The conduction band bottom is located at the K point for all the materials.

We next study the $\Gamma$ point whose point group is $D_{3d}$. The highest occupied level calculated from non-SOC calculations is $E_g$ ($\Gamma_3^+$) and the SOC splits it into $e_{3/2g}(1)$ ($\Gamma_4^+$), $e_{3/2g}(2)$ ($\Gamma_5^+$) and $E_{1/2g}$ ($\Gamma_6^+$) levels according to the direct product:

$$E_g \ (\Gamma_3^+) \otimes E_{1/2g} \ (\Gamma_6^+) = e_{3/2g}(1) \ (\Gamma_4^+) \oplus e_{3/2g}(2) \ (\Gamma_5^+) \oplus E_{1/2g} \ (\Gamma_6^+), \quad (19)$$

where $\Gamma_4^+$ and $\Gamma_5^+$ have the same energy. We find that the $\Gamma_6^+$ level is lower than the $\Gamma_4^+$ and $\Gamma_5^+$ levels. In the Mulliken notation, $E_{3/2g}$ is assigned to the one-dimensional IR, $\Gamma_4^+$ and $\Gamma_5^+$. Therefore, we introduce the notation of $e_{2/3g}(1)$ and $e_{2/3g}(2)$ to represent $\Gamma_4^+$ and $\Gamma_5^+$, respectively.

The $k$-point group on the T and T' ($\Sigma$) lines is $C_2$ ($C_s$). In these cases, each pair of bands have the same energy and belong to $\Gamma_3$ and $\Gamma_4$. These pairing of the bands is due to the time-reversal symmetry. The different degenerate bands do not cross each other. In the case of non-SOC calculations, A or B (A' or A'') are assigned to the bands on the T and T' ($\Sigma$) lines and the two bands belonging to A and B (A' and A'') cross.

7

*3.5. $Z_2$ invariant*

[210] We calculate the $Z_2$ invariants $v$ of the present systems having the inversion symmetry[42]:

$$(-1)^v = \prod_i \delta_i, \tag{20}$$

where $i$ runs over the time-reversal invariant momenta, namely $\Gamma$ and three M points. $\delta_i$ is given by:

$$\delta_i = \prod_{c=1}^{N_{occ.}/2} \xi_{2c}(\vec{k}_i), \tag{21}$$

where $\xi_{2c}(\vec{k}_i)$ is the parity of the $2c$-th band at the point $\vec{k}_i$ and $N_{occ.}$ is the [215] number of the occupied bands. When $v = 1$, the system is identified as a topological insulator.

Table 2 presents results of the analysis. In the Bethe symbols, $+$ and $-$ correspond to the parities of even and odd, respectively, whereas $g$ and $u$ in Mulliken symbols correspond to even and odd, respectively.

[220] Two levels in every Kramers pair at the $\Gamma$ and M points have the same energy and the same parity: $\xi_{2c}(\vec{k}_i) = \xi_{2c-1}(\vec{k}_i)$. We here confirm the same parity by analyzing IR. In the case of the planar structure, every Kramers pair belongs to two-dimensional IR and has the same parity (Table 2). On the other hand, some Kramers pairs belong to different one-dimensional IR in the case of [225] buckled structures. For example, every pair at the M point belongs to $M_1^+$ and $M_2^+$ or to $M_1^-$ and $M_2^-$[43]. Every pair is found to have the same parity. As mentioned in a previous subsection 3.4, we also find that the highest occupied levels at the $\Gamma$ point are paired ($\Gamma_4^+$ and $\Gamma_5^+$ are paired) and every Kramers pair has the same parity.

[230] In all systems, $\delta_i$ are -1 and +1 at the $\Gamma$ and M points, respectively. As a result, $v = 1$, indicating that the systems are topological insulators[44]. The present analysis of topological invariants is possible for two and three dimensional materials having the inversion symmetry.

## 4. Conclusions

[235] We propose a method that identifies IR of the SOC wavefunctions by using computers and apply it to analyze band structures of group-IV two-dimensional systems. The Dirac cone of planar and buckled structures belong to the two-dimensional IR, $E''$ and E, respectively. The SOC splits them into $E_{1/2}$ ($K_7$) and $E_{3/2}$ ($K_9$) in the case of planar structure. We discuss why the $E_{3/2}$ level is lower [240] than the $E_{1/2}$ level by using a tight binding model and find that $\exp(i\vec{k} \cdot \vec{R}_n)$ in the Bloch function affects the identification of IR. In the case of buckled structures, the SOC splits Dirac cone into the higher level of $E_{1/2}$ ($K_6$) and lower two levels of $e_{3/2}(1)$ ($K_4$) and $e_{3/2}(2)$ ($K_5$). The latter two levels have the same energy because of the time-reversal symmetry. We confirm that the $Z_2$ [245] invariants are 1 for all the systems.

## 5. Acknowledgment

[1] K. S. Novoselov, A. K. Geim, S. V. Morozov, D. Jiang, Y. Zhang, S. V. Dubonos, I. V. Grigorieva, A. A. Firsov, Science 306 (5696) (2004) 666–669.

[2] A. Geim, K. Novoselov, Nat. Mater. 6 (2007) 183191.

[3] P. Vogt, P. De Padova, C. Quaresima, J. Avila, E. Frantzeskakis, M. C. Asensio, A. Resta, B. Ealet, G. Le Lay, Phys. Rev. Lett. 108 (2012) 155501.

[4] S. Huang, W. Kang, L. Yang, Appl. Phys. Lett 102 (13) (2013) 133106.

[5] K. Takeda, K. Shiraishi, Phys. Rev. B 50 (1994) 14916–14922.

[6] E. Bianco, S. Butler, S. Jiang, O. D. Restrepo, W. Windl, J. E. Goldberger, ACS Nano 7 (5) (2013) 4414–4421.

[7] F. Zhu, W. Chen, Y. Xu, C. Gao, D. Guan, C. Liu, D. Qian, S. Zhang, J. Jia, Nat. Mater. 14 (2015) 10201025.

[8] L. Chen, C.-C. Liu, B. Feng, X. He, P. Cheng, Z. Ding, S. Meng, Y. Yao, K. Wu, Phys. Rev. Lett. 109 (2012) 056804.

[9] C.-L. Lin, R. Arafune, K. Kawahara, M. Kanno, N. Tsukahara, E. Minamitani, Y. Kim, M. Kawai, N. Takagi, Phys. Rev. Lett. 110 (2013) 076801.

[10] S. Balendhran, S. Walia, H. Nili, S. Sriram, M. Bhaskaran, Small 11 (6) (2015) 640–652.

[11] Y. Yao, F. Ye, X.-L. Qi, S.-C. Zhang, Z. Fang, Phys. Rev. B 75 (2007) 041401.

[12] M. Gmitra, S. Konschuh, C. Ertler, C. Ambrosch-Draxl, J. Fabian, Phys. Rev. B 80 (2009) 235431.

[13] M. Ezawa, J. Phys. Soc. Jpn. 84 (12) (2015) 121003.

[14] M. Ezawa, J. Supercond. Nov. Magn. 28 (2015) 12491253.

[15] F. Matusalem, D. Koda, F. Bechstedt, M. Marques, L. K. Teles, Sci. Rep. 7 (2017) 15700.

[16] S. Minami, I. Sugita, R. Tomita, H. Oshima, M. Saito, Jpn. J. Appl. Phys. 56 (10) (2017) 105102.

[17] E. Kogan, V. U. Nazarov, V. M. Silkin, M. Kaveh, Phys. Rev. B 89 (2014) 165430.

[18] E. Kogan, Graphene 2 (2) (2013) 74–80.

[19] D. Kochan, S. Irmer, J. Fabian, Phys. Rev. B 95 (2017) 165415.

[20] N. A. P. Namari, M. Saito, Jpn. J. Appl. Phys. 58 (6) (2019) 061003.

[21] M. Y. H. Widianto, H. P. Kadarisman, A. M. Yatmeidhy, M. Saito, Jpn. J. Appl. Phys. 59 (7) (2020) 071001.

[22] A. Zaharo, A. Purqon, T. Winata, M. Saito, Jpn. J. Appl. Phys. 59 (7) (2020) 071006.

[23] M. Y. H. Widianto, A. Zaharo, N. A. P. Namari, M. Saito, Jpn. J. Appl. Phys. 60 (6) (2021) 061001.

[24] T. Inui, Y. Tanabe, Y. Onodera, Group Theory and Its Applications in Physics, Springer-Verlag, Tokyo, 1990.

[25] T. Yamasaki, A. Kuroda, T. Kato, J. Nara, J. Koga, T. Uda, K. Minami, T. Ohno, Comput. Phys. Commun. 244 (2019) 264–276.

[26] D. Vanderbilt, Phys. Rev. B 41 (1990) 7892–7895.

[27] P. E. Blöchl, Phys. Rev. B 50 (1994) 17953–17979.

[28] N. Troullier, J. L. Martins, Phys. Rev. B 43 (1991) 1993–2006.

[29] G. Koster, Solid State Phys. 5 (1957) 173–256.

[30] R. S. Mulliken, J. Chem. Phys. 23 (11) (1955) 1997–2011.

[31] R. S. Mulliken, J. Chem. Phys. 24 (5) (1956) 1118–1118.

[32] G. Herzberg, Electronic Spectra and Electronic Structure of Polyatomic Molecules, Van Nostrand, New York, 1966.

[33] J. P. Perdew, K. Burke, M. Ernzerhof, Phys. Rev. Lett. 77 (1996) 3865–3868.

[34] M. Kurpas, P. E. Faria Junior, M. Gmitra, J. Fabian, Phys. Rev. B 100 (2019) 125422.

[35] J. C. Boettger, S. B. Trickey, Phys. Rev. B 75 (2007) 121402.

[36] S. Konschuh, M. Gmitra, J. Fabian, Phys. Rev. B 82 (2010) 245412.

[37] J. McClure, Y. Yafet, in: Proceedings of the Fifth Conference on Carbon, Vol. 1, Pergamon, New York, 1962, pp. 22–28.

[38] J. C. Slater, G. F. Koster, Phys. Rev. 94 (1954) 1498–1524.

[39] Since $\hat{C}_3$ has the same character for the states of $|m_j| = 5/2$ and $|m_j| = 1/2$, we cannot determine whether the two functions belong to $E_{1/2}$ or $E_{5/2}$ in the present analysis but Eq. (7) excludes the possibility of $E_{5/2}$. We can also confirm this identification by examining the operation $IC_6$ which has different characters for $E_{1/2}$ and $E_{5/2}$, where I represents inversion.

[40] C.-C. Liu, W. Feng, Y. Yao, Phys. Rev. Lett. 107 (2011) 076802.

[41] C.-C. Liu, H. Jiang, Y. Yao, Phys. Rev. B 84 (2011) 195430.

[42] L. Fu, C. L. Kane, Phys. Rev. B 76 (2007) 045302.

[43] The Mulliken symbol $E_{1/2g}$ ($E_{1/2u}$) corresponds to $M_1^+$ and $M_2^+$ ($M_1^-$ and $M_2^-$). Since $M_1^+$ and $M_2^+$ ($M_1^-$ and $M_2^-$) are one-dimensional IR, we introduce $e_{1/2g}(1)$ and $e_{1/2g}(2)$ ($e_{1/2u}(1)$ and $e_{1/2u}(2)$) to represent $M_1^+$ and $M_2^+$ ($M_1^-$ and $M_2^-$), respectively.

[44] The present definition of the unit cell (Fig. 1) leads to the fact that $\delta_i$ is $+1$ for the three M points. A previous report on graphene pointed out that the three M points are inequivalent when the definition is changed[42].

12

Table 1: Optimize lattice constant ($a$) and buckling height ($h$) and SOC band gap.

| Material | $a$ (Å) | $h$ (Å) | Band gap (meV) |
|---|---|---|---|
| Graphene | 2.48 | - | 0.5 |
| Silicene | 3.83 | 0.45 | 2 |
| Germanene | 4.06 | 0.64 | 40 |
| Stanene | 4.68 | 0.83 | 65 |

Table 2: Analysis of $Z_2$ invariant. $\xi$ represents the parity and $\delta$ is defined in Eq. (21). The band number in the ascending order of energy corresponds to $c$ in Eq. (21).

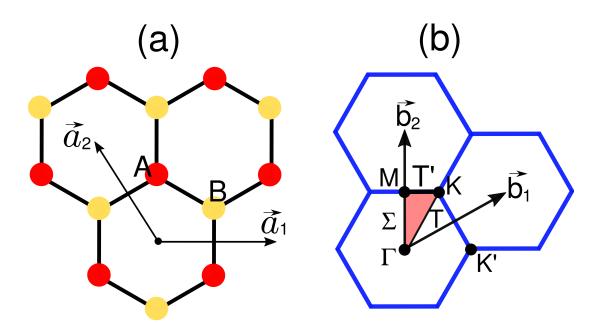| System | $k$-point | Band number | IR | $\xi$ | $\delta$ |
|---|---|---|---|---|---|
| Planar structure | $\Gamma$ (D$_{6h}$) | 4 | E$_{5/2g}$ ($\Gamma_9^+$) | +1 | |
| | | 3 | E$_{3/2g}$ ($\Gamma_8^+$) | +1 | -1 |
| | | 2 | E$_{1/2u}$ ($\Gamma_7^-$) | -1 | |
| | | 1 | E$_{1/2g}$ ($\Gamma_7^+$) | +1 | |
| | M (D$_{2h}$) | 4 | E$_{1/2g}$ (M$_5^+$) | +1 | |
| | | 3 | E$_{1/2u}$ (M$_5^-$) | -1 | +1 |
| | | 2 | E$_{1/2g}$ (M$_5^+$) | +1 | |
| | | 1 | E$_{1/2u}$ (M$_5^-$) | -1 | |
| Buckled structure | $\Gamma$ (D$_{3d}$) | 4 | e$_{3/2g}$(1)(2) ($\Gamma_4^+$ $\Gamma_5^+$) | +1 | |
| | | 3 | E$_{1/2g}$ ($\Gamma_6^+$) | +1 | -1 |
| | | 2 | E$_{1/2u}$ ($\Gamma_6^-$) | -1 | |
| | | 1 | E$_{1/2g}$ ($\Gamma_6^+$) | +1 | |
| | M (C$_{2h}$) | 4 | e$_{1/2g}$(1)(2) (M$_1^+$ M$_2^+$) | +1 | |
| | | 3 | e$_{1/2u}$(1)(2) (M$_1^-$ M$_2^-$) | -1 | +1 |
| | | 2 | e$_{1/2g}$(1)(2) (M$_1^+$ M$_2^+$) | +1 | |
| | | 1 | e$_{1/2u}$(1)(2) (M$_1^-$ M$_2^-$) | -1 | |

Figure 1: Top view of unit cell where red and yellow circles indicate the A and B sublattices, respectively (a) and FBZ (b). Periodic lattice vectors (primitive reciprocal lattice vectors) are denoted as $\vec{a}_1$ and $\vec{a}_2$ ($\vec{b}_1$ and $\vec{b}_2$).
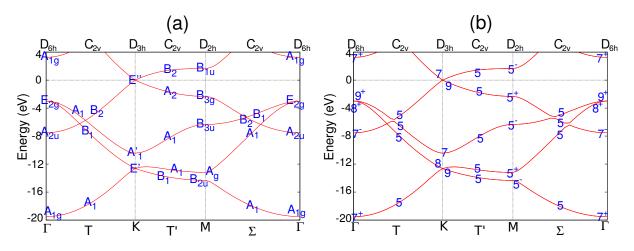


Figure 2: Band structure of graphene calculated from the non-SOC (a) and SOC (b) calculations. The energies are measured from the valence band top energy. In (b), the natural number and the sign (+ and -) indicates the number in the Bethe symbol and the parity, respectively.
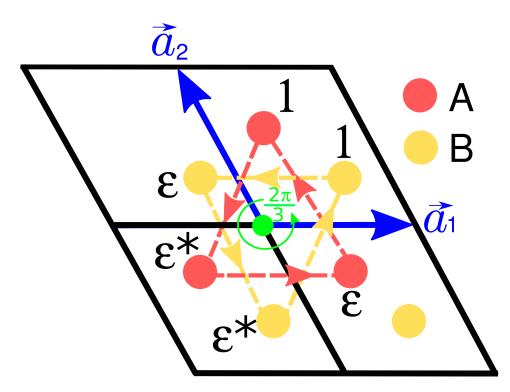
Figure 3: The values of the term $\exp(i\vec{k} \cdot \vec{R})$ for each cell. The green circle arrow indicates the rotation of $\frac{2\pi}{3}$ around the green dot. This rotation transforms the A and B sublattices as indicated by orange and yellow arrows, respectively.
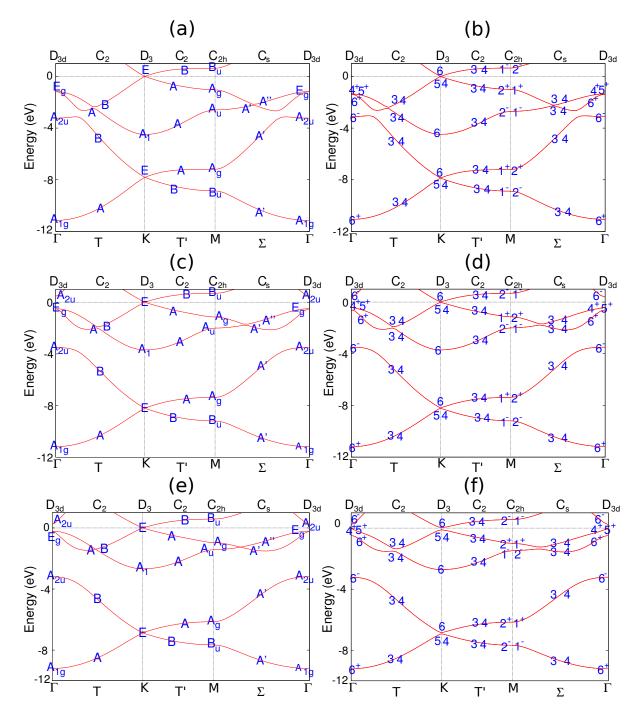
Figure 4: Band structures of silicene (the upper row), germanene (the middle row) and stanene (the lower row). The structures are obtained from non-SOC (the left-hand side) and SOC (the right-hand side) calculations. The energies are measured from the valence band top energy. On the right hand side, the natural number and the sign (+ and -) indicates the number in the Bethe symbol and the parity, respectively.